Kinetic coefficient of Ni solid-liquid interfaces from molecular-dynamics simulations

D. Y. Sun* and M. Asta
Department of Materials Science and Engineering, Northwestern University, Evanston, Illinois 60208, USA

J. J. Hoyt
Sandia National Laboratories, MS 1411, Albuquerque, New Mexico 87185, USA

(Received 15 July 2003; published 28 January 2004)

The kinetics of isothermal crystallization and melting are studied for elemental Ni employing nonequilibrium molecular-dynamics simulations based on interatomic potentials of the embedded-atom-method form. These simulations form the basis for calculations of the magnitude and crystalline anisotropy of the kinetic coefficient μ, defined as the constant of proportionality between interface velocity and undercooling. We obtain highly symmetric rates for crystallization and melting, from which we extract the following values of μ for low index {100}, {110}, and {111} interfaces: $\mu_{100}=35.8\pm22$, $\mu_{110}=25.5\pm1.6$, and $\mu_{111}=24.1\pm4.0$ in units of cm/s K. The results of the present study are discussed in the context of previous molecular-dynamics simulations for related systems, and kinetic models based upon transition-state and density-functional theories.

DOI: 10.1103/PhysRevB.69.024108 PACS number(s): 64.70.Dv, 68.08.−p, 81.30.Fb

I. INTRODUCTION

The kinetic coefficient μ of a molecularly rough solid-liquid interface is the constant of proportionality between growth velocity and undercooling. For metallic systems the magnitude and associated crystalline anisotropy of μ are known to be critical factors governing crystallization rates and growth morphologies under rapid solidification conditions (e.g., Refs. 1–6). To date few direct measurements of μ are available experimentally,[7,8] and much of the current theoretical understanding of crystal-melt interface kinetics has been derived from atomic-scale molecular-dynamics (MD) and Monte Carlo simulations.[9–26]

In the pioneering MD work of Broughton, Gilmer, and Jackson,[9] crystal-growth simulations for Lennard-Jones {100} interfaces yielded appreciable crystallization rates even at very low temperatures where the liquid diffusivity is negligible. These results were thus found to be inconsistent with transition-state theories of growth kinetics in which adatom attachment to the growing solid is modeled as a thermally activated (diffusion-limited) process.[26–29] The results of Broughton *et al.* were however consistent with the observations of Turnbull and co-workers,[30,31] suggesting that crystallization kinetics for pure metals are governed not by diffusive time scales, but rather the frequency of adatom ''collisions'' with the crystal-growth surface. Based on their MD results, Broughton *et al.* formulated a model of collision-limited growth with parameters adjusted to fit the Lennard-Jones MD data. The Broughton-Gilmer-Jackson growth model has been shown to yield values for μ consistent with experimental measurements in Pb (Ref. 8) and MD simulations for a number of face-centered-cubic (fcc) forming metals.[24]

In the context of macroscopic crystal growth, an important result from MD simulations is the finding of appreciable crystalline anisotropy in μ. For the Lennard-Jones system, Burke *et al.* found that {111} interfaces grow at rates two to three times slower than {100}. Comparable anisotropies have been derived in more recent simulation studies for {100}, {110}, and {111} interfaces in the Lennard-Jones system[17] as well as the metals Ni, Ag, Au, and Cu.[19,24,23] For each of these fcc-forming systems the fastest and slowest growth rates in MD are obtained for {100} and {111} orientations, respectively, with kinetic anisotropies spanning the range $\mu_{100}/\mu_{110}\approx1.4$–$1.8$ and $\mu_{111}/\mu_{100}\approx2.0$–$3.6$. In recent quantitative phase-field simulations of dendritic solidification for elemental Ni, Bragard *et al.*[6] demonstrated that kinetic anisotropies of this magnitude play a dominant role in the selection of growth morphologies and dendrite tip velocities at high undercoolings. As discussed in the final section, several alternative models have been proposed to explain the dependence of μ on crystallographic orientation and at present a clear consensus is lacking concerning the dominant microscopic sources of kinetic anisotropy for molecularly rough solid-liquid interfaces.

In the present work we have undertaken a detailed study of the kinetic coefficient of elemental Ni employing MD simulations based upon embedded-atom-method (EAM) interatomic potentials.[32–35] This study follows upon our earlier MD investigations of crystallization kinetics[19,24] for a variety of EAM metals including Ni. The present work was motivated largely by the results of the recent phase-field calculations of Bragard *et al.*[6] demonstrating a high level of sensitivity in predicted Ni dendrite growth velocities and morphologies to relatively small uncertainties in the anisotropy of μ. In the current work we focus on computing refined estimates of μ for {100}, {110}, and {111} interfaces directly in the regime of low undercoolings relevant for the modeling of dendrite growth.[36] This work includes a comparison of results derived from separate nonequilibrium MD (NEMD) methods, and an analysis of the effects upon calculated growth rates arising from choices of system size and dynamical ''thermostat'' and ''piston mass'' variables. Interface velocities are also calculated for both positive and negative undercoolings in order to investigate the generality of a

recent result by Celestini and Debierre[23] featuring appreciable asymmetry between melting and growth kinetics for EAM Au.

The remainder of the paper is organized as follows. The following section includes results of calculated melting properties for the EAM potentials considered in this work. Details of the NEMD simulations, and calculated crystallization and melting kinetics are presented in Sec. III. The results of the present MD studies are subsequently discussed in the context of alternative theoretical models for the magnitude and crystalline anisotropy of μ. The conclusions drawn from this work are summarized in Sec. V.

II. CALCULATED MELTING PROPERTIES

The present simulations are based upon the Foiles, Baskes, and Daw (FBD), Ref. 34, EAM potential for Ni, which yields equilibrium melting properties (see below) and liquid structure factors[37] in very reasonable agreement with experimental data. As will be made clear below, the approaches used to derive μ by NEMD simulations require precise values for the equilibrium melting temperature T_M. In this section we describe our procedure for calculating T_M by MD using a slight modification of the coexistence approach introduced by Morris and co-workers[38,39] (see also Ref. 40). In these and all other simulations described in the following, we have employed the DYNAMO (Ref. 41) and PARADYN (Ref. 42) serial and parallel MD codes. Equations of motion for all simulations have been integrated using a predictor-corrector algorithm[43] with time steps of 0.002 or 0.003 ps.

To derive melting temperatures we begin by performing standard *N-P-T* (constant number, pressure, and temperature ensemble) MD simulations to determine the equilibrium (zero-pressure) lattice parameter of the bulk fcc crystal as a function of temperature. Subsequently, we equilibrate a crystalline simulation cell at a temperature and lattice constant corresponding to our initial estimate of T_M. Half of the atoms in the cell are subsequently melted using constant-volume simulations with half of the atoms fixed and the others maintained at temperatures approximately 1000 K above T_M employing a Nosé-Hoover thermostat[44,45] or Monte Carlo simulation. This procedure results in a periodic two-phase solid-liquid simulation cell containing two crystal-melt interfaces. Keeping the solid atoms fixed, the liquid is subsequently equilibrated at the estimated melting temperature, allowing the cell length normal to the interfaces to adjust to minimize stress. This equilibration phase is typically performed with simulations lasting on the order of 500 ps. Next, the entire system is allowed to relax employing canonical-ensemble (fixed *N*, *T*, and volume) simulations lasting up to 1 ns with the temperature maintained at the estimated value of T_M. A refined estimate of T_M is then derived employing Andersen-Parinello-Rahman dynamics[46–49] with no imposed temperature thermostat. In these simulations the periodic dimensions parallel to the solid-liquid interfaces are held fixed, while the length normal is allowed to evolve dynamically with zero imposed stress. The refined estimate of T_M is derived from the average temperature measured from such coexistence simulations lasting up to several nanoseconds. The dimensions of the simulation cell are subsequently scaled to the appropriate value of the crystal lattice constant corresponding to the new estimate of T_M, and an additional coexistence simulation is performed to refine the value of the melting temperature further. This process is iterated until the coexistence temperature is derived corresponding to zero stress in the bulk crystal and liquid phases, giving our final estimated value of T_M.

TABLE I. Melting temperatures T_M derived from coexistence simulations employing varying cell sizes and interface orientations. The notation for system size is described in the text. For the calculated melting temperatures, error bars denote 95% confidence intervals.

Orientation	Size	Number of particles	T_M(K)
(100)	$10\times10\times100$	10000	1714.4 ± 2.8
(100)	$15\times15\times100$	22500	1712.6 ± 4.0
(110)	$8\times10\times120$	9600	1701.1 ± 5.6
(111)	$10\times10\times99$	9900	1720.1 ± 2.4
(111)	$20\times20\times99$	39600	1707.6 ± 1.4

Table I reports values of T_M derived from the coexistence approach using each of the cell geometries employed in the NEMD simulations described below. The geometries of these different cells are denoted as follows. For each cell (hkl) refers to the orientation of the solid-liquid interfaces. For (001), $(10\times10\times100)$ and $(15\times15\times100)$ correspond to cells with periodic lengths that are respectively 10 and 15 fcc nearest-neighbor spacings in length along the x and y (fcc $[1\bar{1}0]$ and $[110]$) directions parallel to the interface; prior to melting the initially crystalline cell contains 100 layers along the normal direction z. Similarly for (111), $(n\times n\times99)$ cells are n nearest-neighbor spacings in length along x (fcc $[1\bar{1}0]$ direction), n layers in length along y ($[11\bar{2}]$), and contain 99 initially crystalline layers along z ($[111]$). Finally, the $(8\times10\times120)$ cell for (110) has dimensions of 8 times the fcc lattice constant along x ($[001]$), 10 times the nearest-neighbor distance along y ($[1\bar{1}0]$), and 120 initially crystalline layers in z. Note that, for (001) and (111) interface orientations, simulation cells with two different dimensions are considered to investigate system-size effects in the calculations for μ (see below).

The values of T_M reported in Table I show slight variations (up to $\approx$20 K or about 1%) with cell size and interface orientation. These differences reflect the magnitude of the size effects associated with our approach for computing T_M. In particular, we have found for related systems that the variation of the calculated melting temperatures with interface orientation can be minimized by enlarging the lateral size of the simulation cell. From the average of the results in Table I we estimate a bulk zero-pressure melting temperature for the FBD Ni potential of $T_M\approx1710\pm10$ K. This value is in reasonable agreement with previous values of T_M calculated for the same potential: Foiles and Adams obtained $T_M=1740$ K employing a thermodynamic integration method,[50] while Chen, Barnett, and Landman derive $T_M=1733$

TABLE II. Comparison of calculated and experimentally measured (Ref. 56) melting properties for Ni.

	T_M(K)	L(eV/atom)	$\Delta\omega$(Å^3/atom)
Calculated	1710	0.18	0.867
Experiment	1726	0.181	0.67

± 22 K.[51] Table II provides a comparison between our calculations and experimentally measured melting properties including T_M, the latent heat per atom (L), and the volume change on melting: $\Delta\omega=\omega_l-\omega_s$, where ω_s and ω_l denote atomic volumes in the solid and liquid phases, respectively.

In the following section we employ a NEMD method for extracting μ from measured crystallization (or melting) velocities resulting from imposed stress P_n normal to the solid-liquid interface. The implementation of this method requires a knowledge of the variation of T_M as a function of P_n, which can be derived readily using the same coexistence approach described above. Specifically, starting with the solid-liquid cells equilibrated with zero imposed stress we perform additional coexistence simulations with nonzero values of an externally imposed P_n, and determine the value of $T_M(P_n)$ from the resulting average temperature. Results are shown in Fig. 1 which plots T_M vs P_n for the three different interface orientations. For each simulation cell a linear relation (within statistical uncertainty) is obtained consistent with the behavior expected from the Clausius-Clapeyron relation. The offsets of the different lines (and most likely the apparent differences in slope as well) reflect the aforementioned finite-size effects.

III. SIMULATIONS OF MELTING AND GROWTH KINETICS

Under isothermal conditions, the kinetic coefficient μ is defined as the proportionality constant between the velocity V of a solid-liquid interface and its undercooling $[\Delta T=T-T_M(P)]$:

$$V(T)=\mu[T-T_M(P)], \tag{1}$$

where T and P denote the temperature and imposed pressure, respectively, and $T_M(P)$ is the pressure-dependent melting temperature. From the structure of Eq. (1), several alternative NEMD approaches can be formulated for the calculation of μ. For example, one can impose a temperature T above or below T_M to a solid-liquid system, and measure the resulting interface velocity to extract μ. This approach, which has been implemented by a number of authors previously,[16–21,24] will be referred to below as the *free solidification* (FS) method. Alternatively, one can maintain the temperature of a solid-liquid system at the zero-pressure melting point $[T_M(P=0)]$ and impose a finite external normal stress, resulting in a modified melting temperature (cf., Fig. 1), a finite ΔT, and associated interface growth or melting. This approach will be referred to as the *imposed pressure* (IP) method. While FS and IP methods are formally related, the details surrounding their implementation in NEMD simulations are clearly different. A comparison of the results derived from these different approaches thus serves as a check on the accuracy of the assumptions underlying the application of the NEMD methods. In the following sections we present a detailed discussion of our implementation of the FS and IP methods, and show that the two give results for μ in good agreement in their application to EAM Ni.

In the present work we have also investigated a third NEMD for calculating μ based on Eq. (1), involving the imposition of forced interface velocities. In this *forced velocity* (FV) method, the periodic length of the simulation cell normal to the solid-liquid interface is uniformly scaled to produce a constant rate of change of the volume of the solid-liquid system while the temperature is maintained at the zero-pressure melting point. As the volume is scaled, the pressure in the system builds up and simultaneously crystallization or melting commences. Eventually, the system is observed to approach a steady-state condition in which the imposed volume scaling is compensated by the rate of crystallization or melting. The corresponding driving force for this interface motion can then be derived from the steady-state average value of the pressure, which is converted to an effective undercooling using the Clausius-Clapeyron relation (Fig. 1). While the FV method was found to yield growth and melting rates consistent with the FS and IP methods, much longer equilibration times were required to achieve steady-state kinetics with this approach (presumably due to the fact that the constant scaling of volume suppresses density fluctuations allowed in the FS and IP methods). Due to these long equilibration times it was difficult to ascertain whether steady-state conditions were realized in the simulations, and calculated growth velocities featured relatively high statistical uncertainties. For these reasons, the FV approach is viewed to be less practical than either the FS or IP NEMD methods.

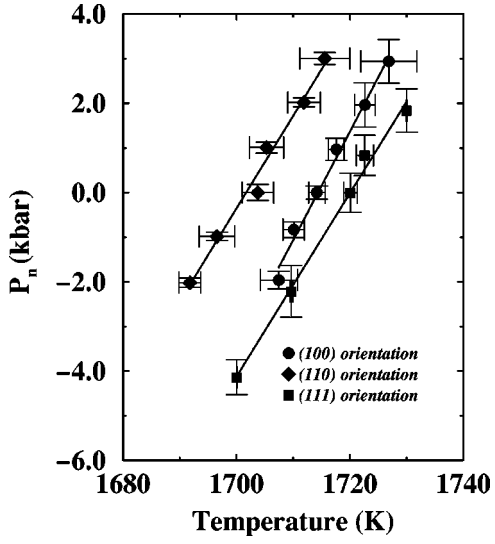

FIG. 1. Calculated melting temperatures as a function of imposed stress P_n normal to the solid-liquid interfaces. The circles are the MD results, and the line represents a least-squares fit to the data.

A. Dynamics and initial conditions

Free-solidification and imposed-pressure results have been received employing simulations in an $NTAP_n$ ensemble corresponding to constant values of the particle number (N) and temperature (T), as well as the area A parallel and stress P_n normal to the solid-liquid interfaces. These simulations employ the well-known equations of motion formulated by Andersen,[46] Parinello and Rahman,[47–49] Nosé,[44] and Hoover,[45] which introduce extra dynamical variables associated with thermal inertia Q and piston mass M. In the application of these equations of motion to calculations of μ, it is important to check that computed growth velocities are insensitive to the choice of these dynamical variables. We present below a comparison of results for μ derived from a few different choices of Q and M, and for the following it is thus useful to clarify the definition of these parameters by providing explicit expressions for the equations of motion employed in the current simulations.

Let L_α ($\alpha=x,y,z$) denote the periodic lengths of an orthorhombic simulation cell. The position of each particle (i) is given in scaled coordinates by $s^i_\alpha = r^i_\alpha / L_\alpha$. The equations of motion for s^i_α and L_α read (where dots denote time derivatives)

$$\ddot{s}^i_\alpha = \frac{f^i_\alpha}{mL_\alpha} - \left(2\frac{\dot{L}_\alpha}{L_\alpha} + \xi\right)\dot{s}^i_\alpha, \tag{2}$$

$$\ddot{L}_\alpha = \frac{(P_\alpha - P^0_\alpha)\Omega}{ML_\alpha}, \tag{3}$$

where $\mathbf{f}^i$ is the interatomic force on particle i, m is the particle mass, Ω denotes the volume of the simulation cell, and P_α and P^0_α are the instantaneous and imposed values of the stress along the normal direction α, respectively.[52] M and ξ in Eqs. (2) and (3) denote the piston mass and thermostat friction coefficient, respectively. In the Nosé-Hoover scheme, the equation of motion for the latter can be written as

$$\dot{\xi} = \frac{T - T_0}{Q}, \tag{4}$$

where Q is the thermal inertia, and T and T_0 denote instantaneous and imposed values of the temperature, respectively. For most of the present simulations M and Q are set as 100 eV ps^2/Å^2 and 200 K ps^2, respectively, although results are also presented below using slightly different values to investigate whether the final calculations for μ are sensitive to their choice.

All of the simulations of crystal growth and melting presented below have been performed using, as initial conditions, simulation cells prepared as follows. We begin with solid-liquid systems equilibrated at the zero-pressure melting point employing the approach described in Sec. II above. We then prepare initial cells for growth (melting) simulations containing approximately 15% crystal (liquid) and 85% liquid (crystal) by slowly melting (growing) the crystal using free-solidification simulations performed roughly 5 K above (below) the equilibrium melting point. The resulting systems

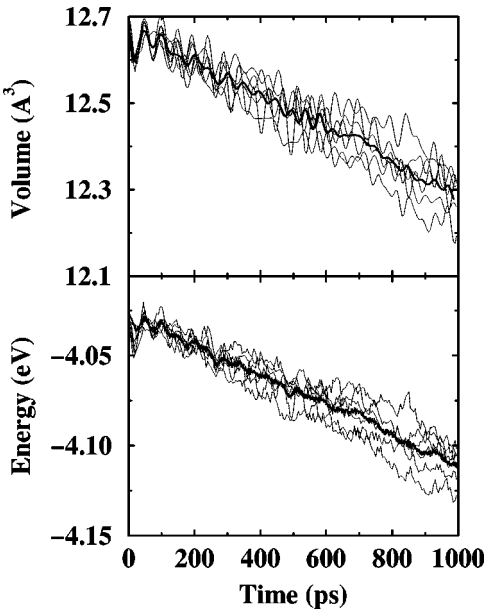

FIG. 2. The volume per atom (upper panel) and potential energy per atom (lower panel) as a function of time during a free solidification simulation for a {100} oriented interface with 10 000 particles. The thin lines represent results from six independent runs, while the thick lines are averages.

are subsequently equilibrated for 300 ps at the melting temperature. Six different configurations are extracted during this equilibration phase (50 ps apart) which provide the initial atomic positions for subsequent NEMD simulations of melting or growth. From these starting structures we initiate melting or growth by (instantaneously) changing either temperature or pressure as described below. Consequently, some time is required for the liquid and solid structures to equilibrate after these sudden ''quenches.'' A transient period is thus observed in the subsequent isothermal simulations, before the system reaches steady-state growth or melting (see below). At this point it is therefore important to emphasize an important aspect of the present work, namely, the use of very small values ($\Delta T/T_M < 2\%$) for undercooling/superheating. With these small undercoolings, the systems remain close to equilibrium at the initiation of the growth/melting simulations. This allows us to avoid the relatively long time scales that have been demonstrated to govern the equilibration of liquid structure in quenching simulations of highly undercooled melts (e.g., Refs. 53–55).

B. Free solidification simulations

Figure 2 shows the results of a typical free-solidification simulation, performed at an undercooling of 10 K for a 10 $\times 10 \times 100$ simulation cell with an (001) oriented solid-liquid interface. The top and bottom panels plot the volume and potential energy of the system (per atom), respectively, as a function of simulation time. The thin solid lines represent results derived from six independent systems, and the solid line is obtained by averaging. Each system displays a similar transient behavior for an initial period of approximately 100 ps, before steady-state growth is observed to set

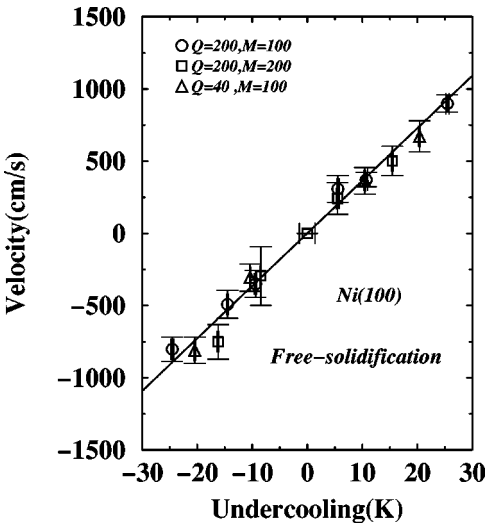

FIG. 3. Velocity versus undercooling results derived from free-solidification simulations for {100} solid-liquid interfaces employing simulation cells with 10 000 particles and three different choices for the dynamical thermostat (Q) and piston-mass (M) parameters. The units for Q and M are given in the text. In this and subsequent figures error bars denote standard errors on the mean values of the measured velocities derived from the six independent simulations, and solid lines correspond to least-squares fits to the data.

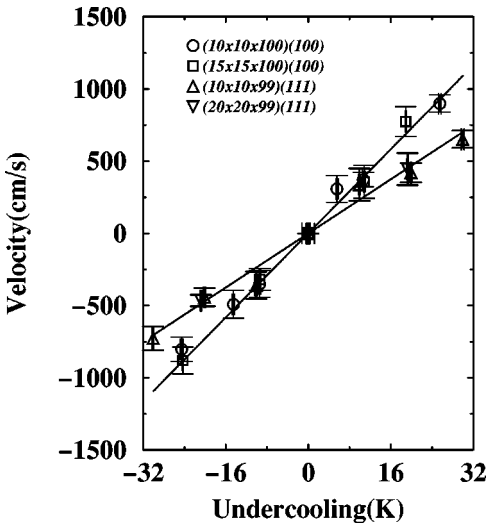

FIG. 4. Velocity versus undercooling results for {100} and {111} interfaces derived from free-solidification simulations employing cells with varying lateral dimensions.

in. During the subsequent solidification of the system, the potential-energy and volume decrease accompanying the growth of the crystal.

From the results plotted in Fig. 2, and a knowledge of the volume and potential-energy differences between bulk solid and liquid phases, the interface velocity V can be readily extracted (e.g., Refs. 17,19). For a given steady-state value of the slope of volume versus time ($\dot{\Omega}$), V is given as

$$V(\Delta T) = \frac{\dot{\Omega} d}{2n(\omega_l - \omega_s)}, \tag{5}$$

where ω_s and ω_l denote volumes per atom for bulk solid and liquid phases, respectively, and the factor of 2 accounts for the presence of two interfaces in the periodic simulation cell. In Eq. (5), d and n denote the interplanar spacing and the number of atoms per layer in the growth plane of the crystal, respectively. $V(\Delta T)$ can also be derived independently from the steady-state slope of the potential energy ($\dot{E}$):

$$V(\Delta T) = \frac{\dot{E}(\omega_l - \omega_s)}{2A(e_l - e_s)}, \tag{6}$$

where A is the cross-sectional area of the simulation cell, and e_s and e_l denote the potential energies (per atom) for bulk solid and liquid, respectively. In the results that follow we have found that Eqs. (5) and (6) give essentially identical values for steady-state interface velocities, consistent with the findings of Huitema *et al.*[17]

Figures 3 and 4 give velocity versus undercooling results for (001) and (111) interfaces derived from FS simulations employing different system sizes and alternate choices for the thermostat and piston-mass variables. In these figures the open symbols are derived from Eqs. (5) and (6) using steady-state values of $\dot{\Omega}$ and $\dot{E}$ averaged over six independent runs for each undercooling. Error bars denote estimated uncertainties (standard errors) in the mean value of V, obtained from the variance of the interface velocities derived separately from each of the six independent simulations for a given ΔT.

In Fig. 3 we show results for (001) oriented interfaces derived from $10\times10\times100$ simulation cells with different choices of the thermostat and piston-mass variables defined in Eqs. (2)–(4). The solid line in Fig. 3 represents a least-squares fit to all of the data. For each set of simulation data a linear relation between V and ΔT is obtained over the range of undercoolings examined. From the slope of the V versus ΔT data in Fig. 3 we obtain the values of μ given in the first three lines of Table III. Within the statistical precision of the simulations, the calculated values of μ are found to be insensitive to the choice of Q and M.

In Fig. 4 we plot velocity-undercooling data derived by FS simulations for (001) and (111) interfaces with varying dimensions of the simulation cell parallel to the solid-liquid

TABLE III. Values for the kinetic coefficient derived from free-solidification (FS) and imposed-pressure (IP) NEMD methods for different interface orientations, system sizes, and choices of thermal inertia (Q) and piston-mass (M) parameters; error bars on μ denote 95% confidence intervals.

Orientation	Size	Q	M	Method	μ(cm/s K)
(100)	(10×10×100)	40	100	FS	35.6±4.5
(100)	(10×10×100)	200	200	FS	38.1±8.3
(100)	(10×10×100)	200	100	FS	35.4±3.1
(100)	(15×15×100)	200	100	FS	37.0±3.0
(100)	(10×10×100)	200	100	IP	38.0±1.8
(110)	(10×8×120)	200	100	IP	25.5±1.6
(111)	(10×10×99)	200	100	FS	24.1±4.0
(111)	(20×20×99)	200	100	FS	22.7±1.2

interface. As in Fig. 3 the results are well described by a linear growth relation. Values of μ extracted from each of the separate datasets are listed in Table III. Comparing the results from $10\times10\times100$ and $15\times15\times100$ simulation cells for (001) interfaces, we see that the calculated values of μ agree to within the estimated statistical uncertainties of 5–10 %. This result is consistent with the findings of Celestini and Debierre,[23] who performed detailed investigations of system size effects in their MD calculations of μ for EAM Au. For {100} interface orientations these authors find that the values of μ derived from systems with cross-sectional areas comparable to those used here are converged with respect to system size to within about 5%.

The last two rows of Table III give values of μ for (111) interfaces calculated with system sizes differing by a factor of 4 in cross-sectional area. As for the (001) orientation, we find no indication of a strong system-size dependence for μ_{111}. Our results for (111) interfaces in Ni are thus in sharp contrast with previous findings for the Lennard-Jones[10] and EAM Au[24,23] systems where large decreases (30–50 %) in MD-calculated values of μ_{111} resulted from comparable increases in the lateral dimensions of the simulation cells. For the Lennard-Jones and Au systems this strong size dependence has been attributed to the presence of stacking-fault islands formed at the growing crystal-melt interface. These defects were first identified by Burke, Broughton, and Gilmer[10] (BBG) in their study of the Lennard-Jones system. To explain the large size effect for (111) interfaces BBG noted that, since the growing crystal remains free of stacking faults, the defective hcp islands must anneal out for the interface to advance. In a system with small periodic lengths parallel to the interface, the defect clusters cannot grow as large before contacting clusters from the periodic image of the cell. BBG argued that, since the cluster circumference–to–area ratio determines the annealing rate, smaller systems should exhibit faster interface growth velocities, consistent with observations for Lennard-Jones and Au systems. In light of this explanation, the absence of a pronounced size effect for μ_{111} in the current results for Ni can be interpreted as a reflection of the much higher stacking fault energy in this system. Specifically, the FBD potentials for Ni predict stacking fault energy (SFE) values (see below) that are roughly a factor of 5 larger than for Au and at least an order of magnitude greater than the Lennard-Jones system; a higher stacking-fault energy should lead to a decrease in the population of defective hcp islands at the growing interface, with a diminished effect upon crystallization kinetics.

To conclude this section we note that the relatively high scatter in the data for the six independent simulations shown in Fig. 2 is qualitatively similar to the results obtained in FS simulations for the Lennard-Jones system by Tepper and Briels.[21] In order to average out such statistical variations these authors perform 50 independent simulations, and are able to identify two distinct regimes of constant growth rate in their simulations: a short-time period of relatively rapid growth that they associate with a period of interface relaxation, followed by a long-time regime associated with macroscopic growth. In the present work for EAM Ni, we find no clear evidence for these distinct growth regimes. This qualitative discrepancy between our results and those of Tepper and Briels may be due to differences in the procedures employed to set up the initial states for the NEMD simulations, or may reflect differences between EAM Ni and Lennard-Jones systems related to the response of the interface to rapid changes in temperature. Another possible explanation for the absence of a short time growth regime in the present EAM Ni simulations is the system-size effect. Tepper and Briels report that the initial growth regime is of a much shorter duration in their large system size (8096 atoms) than was found in the smaller systems (4048 atoms). Presumably the initial growth phase is shorter still in the larger systems studied here and it is possible that the initial growth period lies within the 100 ps transient (see Fig. 2) excluded in our computation of the kinetic coefficient.

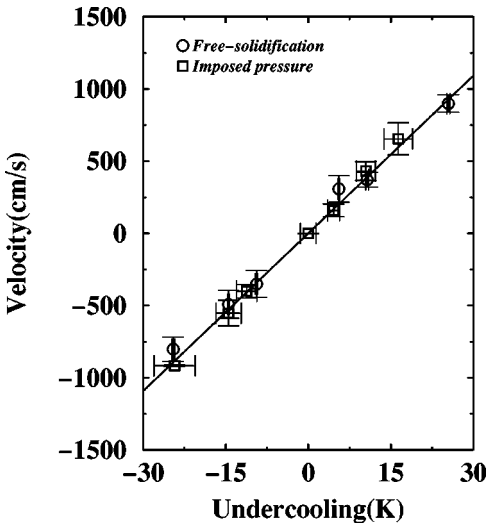

FIG. 5. The interface velocity as a function of undercooling derived from two different nonequilibrium MD methods, imposed pressure (diamonds), and free solidification (squares). Results are for {100} interfaces and were derived from the simulation cells containing 10 000 particles.

C. Imposed-pressure simulations

In the imposed-pressure MD simulations the temperature of the two-phase solid-liquid system is maintained at the zero-pressure melting point while an external stress P_n is imposed normal to the solid-liquid interface. A positive (negative) value of P_n has the effect of raising (lowering) the equilibrium melting temperature, resulting in a finite bulk undercooling ΔT given through the Clausius-Clapeyron relations plotted in Fig. 1, and subsequent crystallization (melting) of the system. The time required for the system to achieve steady-state growth/melting with this method was found to be comparable to that in the FS approach, i.e., approximately 100 ps as shown in Fig. 2. It is important to emphasize that, due to finite-size effects, application of the IP approach requires precise calculations of $T_M(P_n)$ independently for each simulation geometry.

Figure 5 provides a comparison between $V-\Delta T$ results obtained by IP and FS methods for (001) interfaces using $10\times10\times100$ simulation cells. Kinetic coefficients derived

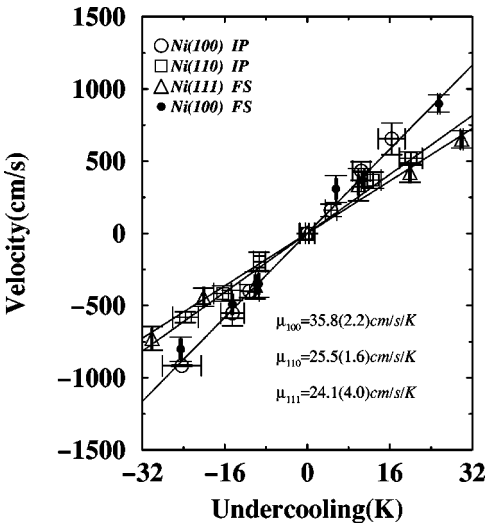

FIG. 6. The interface velocity as a function of undercooling for {100}, {110}, and {111} orientations. Results plotted with open and filled symbols were derived by the free-solidification and imposed-pressure methods, respectively. In the results quoted for μ, 95% confidence intervals on the final significant figure(s) are given in parentheses.

from these two sets of data are given in the third and fifth rows of Table III. The values of μ obtained from the two methods are found to agree to within the estimated error bars, at the level of about 10%. As compared to the FS results, the IP data in Fig. 5 are seen to feature comparable statistical uncertainties in both the values of interface velocity (estimated from the scatter of six independent runs) and undercooling (originating from uncertainties in the slope of the Clausius-Clapeyron relations given in Fig. 1). Nevertheless, with the system sizes and simulation times employed in the present simulations the resulting estimated uncertainties in μ derived by the IP method are found to be comparable to those obtained with the FS approach. The good level of agreement between the FS and IP results provides a nontrivial check on the validity of the assumptions underlying the current application of NEMD methods to the calculation of crystal-melt kinetic coefficients.

Given that the FS and IP methods appear to provide consistent results, it is worthwhile commenting on which of the two methods are preferred in practice. As emphasized above, the IP method requires accurate calculations of the $T_M(P_n)$ relation independently for each simulation geometry considered. By comparison, application of the FS method requires only an estimate of the zero-pressure melting point. In practice, due to the significant computational cost required to compute the $T_M(P_n)$ relation for each simulation cell, FS is clearly preferred over the IP method in NEMD calculations of μ.

IV. DISCUSSION

The final results of our calculations for μ in Ni are summarized in Fig. 6 which plots velocity versus undercooling relations for {100}, {110}, and {111} interface orientations derived from free-solidification and imposed-pressure NEMD methods. These results yield the following values for the kinetic coefficient: $\mu_{100}=35.8\pm2.2$, $\mu_{110}=25.5\pm1.6$, and $\mu_{111}=24.1\pm4.0$ in units of cm/s K, where the error denote 95% confidence intervals bars. For {100} orientations, this value of μ was derived from least-squares fits of V vs ΔT derived from both FS and IP methods using $10\times10\times100$ simulation cells. The values of μ_{110} and μ_{111} were obtained from results of $10\times8\times120$ IP and $10\times10\times99$ FS simulations, respectively. Due to improved statistics and the use of smaller undercoolings in the present work, these results are viewed to be more accurate than our early MD calculations of the kinetic coefficient for Ni which yielded $\mu_{100}=42$, $\mu_{110}=32$, and $\mu_{111}=18$ cm/s K. The currently reported value of μ_{100} is in agreement (within statistical uncertainties) with a value of 39 ± 4 cm/s K quoted in Ref. 57 based upon preliminary results from the current work.

A. Symmetry of melting and growth kinetics

The data in Figs. 3–6 feature highly symmetric results for melting and growth kinetics in the regime of low undercoolings explored in this work. Our results are thus in agreement with those of Tepper and Briels who also obtained symmetric melting and growth kinetics in NEMD simulations for the Lennard-Jones system.[21] The results are also consistent with general arguments based upon microscopic reversibility (e.g., Ref. 58) suggesting that the slope of V versus ΔT should be continuous in the limit of low undercoolings for rough elemental solid-liquid interfaces. Our present data for Ni and that of Tepper and Briels for the Lennard-Jones system are, however, at variance with the MD results of Tymczak and Ray[11,12] for Na and Celestini and Debierre[23] for Au where clear slope discontinuities are obtained in calculated $V-\Delta T$ relations at low undercoolings. In these previous studies melting was found to be faster than solidification by a factor in the range of 1.6–3.6. Based upon their finding that relatively long equilibration times are required to achieve steady-state growth in NEMD simulations of crystal growth, Tepper and Briels argue that the asymmetric kinetics calculated for Na may reflect an artifact associated with the use of small system sizes in the early MD simulations of Tymczak and Ray.[59] This argument is, however, unable to explain the more recent results of Celestini and Debierre who employ a directional-solidification MD scheme that allows simulations of melting and growth to be conducted for times substantially longer than in the present simulations.

To explain the qualitative difference between their results and those of Tepper and Briels, Celestini and Debierre propose that the asymmetric melting and growth kinetics obtained in their simulations reflect a strong tendency towards structural ordering in the Au crystal-melt interface. Celestini and Debierre point out that their simulations were performed employing a many-body ''glue'' potential developed by Ercolessi *et al.*[60] which, relative to Lennard-Jones, is known to enhance tendencies towards structural reconstructions at crystal-vapor and liquid-vapor[61] interfaces. In this respect, it was thus suggested that the discrepancy between the Lennard-Jones and Au results reflect differences in the nature

of the interatomic potentials for these systems. In our current work for Ni we have employed an EAM potential with a form qualitatively similar to the Au glue potential. The discrepancy between our results, featuring highly symmetric melting/growth kinetics for Ni, and those of Celestini and Debierre for Au are thus surprising.

Two possible explanations for the discrepancy between the results for Ni and Au are as follows. First, even though the EAM-Ni potential used here and the glue potential for Au have the same ''pair-functional''[62] form, the latter potential is known to display a more pronounced tendency towards reconstructions at solid-vapor and liquid-vapor surfaces.[63] Hence, it is possible that the asymmetric melting/growth kinetics for Au reflect a stronger tendency towards structural ordering in the solid-liquid interface. A second potential source for the discrepancy between the current results and those of Celestini and Debierre is the presence of large thermal gradients in the latter simulations. The MD approach developed by Celestini and Debierre mimics a directional solidification experiment in which solidification and melting result from ''pulling'' of the solid-liquid system through a thermal gradient. Due to the relatively small systems used in MD simulations, the approach employs thermal gradients on the order of 10^{10} K/m that are many orders of magnitude larger than experiment (with solid-liquid boundary widths of approximately two unit cells, a 10^{10} K/m gradient in Au corresponds to a variation in temperature of roughly 80 K over the interfacial region). High thermal gradients are known to have the effect of suppressing capillary fluctuations,[64,65] and solid-liquid interfaces in the Celestini and Debierre approach are thus expected to be more atomically ''flat'' than those in the NEMD FS simulations employed here (where the application of a thermostat over the entire system leads to highly uniform temperature profiles[21]). Thus, the symmetric melting and growth kinetics obtained in the present simulations, and in the work of Tepper and Briels, are expected to be more representative of the dynamics of rough interfaces. Clearly, further work is required to completely understand the source of the discrepancy between our current results for Ni and those of Celestini and Debierre for Au. For example, it would be of interest to investigate whether the magnitude of the asymmetry between melting and growth rates obtained for Au is sensitive to changes in the magnitude of the thermal gradients employed in the directional-solidification MD simulations.

B. The magnitude of the kinetic coefficient

Broughton, Gilmer, and Jackson (BGJ), Ref. 9, have formulated a model of collision-limited growth kinetics with parameters adjusted to fit velocity vs undercooling MD data for {100} oriented solid-liquid interfaces in the Lennard-Jones system. In the BGJ model, the growth velocity V is related to interface temperature T through an equation motivated by transition-state theory:

$$V(T) = V_0(T)\{1 - \exp[\Delta g(T)/k_B T]\}, \tag{7}$$

where $\Delta g(T)$ is the thermodynamic driving force given as the difference between solid and liquid chemical potentials, and the kinetic prefactor $V_0(T)$ reflects the nature of the microscopic processes governing adatom attachment to the growing crystal. In the BGJ model this term is given by the expression

$$V_0(T) = (d/\lambda)(3k_B T/m)^{1/2} f_0, \tag{8}$$

where $(3k_B T/m)^{1/2}$ is the thermal velocity V_T, d is the interplanar spacing, $\lambda = 0.4a$ is the average distance from the center of points distributed randomly within a sphere of radius equal to the nearest-neighbor spacing a, and f_0 denotes the fraction of favorable growth sites at the interface. The value $f_0 = 0.27$ was found to give the best fit to the MD Lennard-Jones data for the [100] growth direction. At low undercoolings, Eqs. (7) and (8) can be linearized to yield the following expression for the kinetic coefficient:

$$\mu = \frac{d}{\lambda}\frac{L}{k_B T_M^2} V_T f_0. \tag{9}$$

Applying the BGJ model to Ni, using the melting properties for the FBD potentials given in Table II, we obtain from Eq. (9) $\mu = 41$ cm/s K, in reasonably good agreement with the value of 35.8 ± 2.2 cm/s K derived from the present MD results.

An important feature of the BGJ model for collision-limited growth is the proportionality between μ and the thermal velocity. Specifically, V_T is typically much smaller than the speed of sound (V_S) identified by Coriell and Turnbull[31] as an upper bound for V_0 in Eq. (7). The Coriell and Turnbull upper limit, $\mu = V_s L/k_B T_M^2$, is commonly employed as an estimate of the kinetic coefficient in continuum models of dendritic solidification. For Ni, this estimate yields a value of μ that is roughly a factor of 5 larger than that obtained from the present MD calculations and the BGJ model.[19] The scaling of μ with thermal velocity has been derived also within the framework of kinetic density-functional-theory (DFT) models.[66–71]

In the kinetic DFT formulation of Mikheev and Chernov,[66] it is assumed that isothermal solid-liquid interface velocities are governed by the rate of propagation of crystalline ''density waves'' in advance of the moving solid-liquid interface. The model yields the following expression for the kinetic coefficient:

$$\mu = \frac{L}{k_B T_M^2}\frac{S(G_1)\xi_b}{\tau(G_1) N_1 A_s}, \tag{10}$$

where N_1 is the number of reciprocal lattice vectors in the minimal set (e.g., $N_1 = 8$ for fcc) and ξ_b is the correlation length in the liquid, i.e., the inverse half-width of $S(k)$ evaluated at the main peak. A_s is a factor governing the anisotropy of μ (see below). Mikheev and Chernov argue that the unknown terms in Eq. (10) can be replaced by those of the well-studied hard-sphere system. For example, the relaxation time is given by[72] $\tau \approx 1/2(m/k_B T)^{1/2}\sigma$, ξ_b is given by $\approx 1.8\sigma$ and $S(G_1) \approx 2.85$. With the numerical values of the constants provided by the hard-sphere model, Mikheev and Chernov find $\mu_{100} \approx 0.72$ for the Lennard-Jones system as compared

to a value of 1.17 from simulation.[9] For Pb, the model predicts $\mu \approx 14$ cm/s K whereas experiments of Rodway and Hunt[8] yield $\mu = 28 \pm 8$ cm/s K. For EAM Ni, the theory predicts $\mu_{100} \approx 26$ cm/s K whereas the current MD simulations give $\mu_{100} = 35.8 \pm 2.2$ cm/s K. Thus, the theory tends to underestimate by roughly 25–50 % the magnitudes of μ obtained from experiment and MD simulations. It appears that the discrepancy between the Mikheev-Chernov model and the MD simulation results is not due to the hard-sphere approximations. For Ni, using actual values of $S(G_1)$, ξ_b, and τ determined from MD simulations of the bulk liquid, one finds a kinetic coefficient even lower than that predicted from the hard-sphere result. Interestingly, however, the theory predicts kinetic-coefficient anisotropies in reasonable agreement with the present results for Ni as discussed below.

Oxtoby and co-workers have also performed extensive work applying DFT in studies of crystal-growth kinetics.[67–71] In the most recent of these studies, Shen and Oxtoby[71] developed a theory of crystallization and melting kinetics in the Lennard-Jones (LJ) system employing realistic free-energy functionals.[73,74] The functional involves two order parameters: a conserved microscopic density function and a nonconserved parameter defining the local degree of crystallinity. The equations of motion for the former are derived from the nonlinear Navier-Stokes equation,[70] whereas the latter obey a simple relaxational dynamics of the Ginzburg-Landau form. As in the Mikheev and Chernov approach, the mobility parameter entering the equation of motion for the nonconserved order parameter is derived from the relaxation time for density fluctuations in the bulk liquid. Shen and Oxtoby thus develop parameter-free equations of Lennard-Jones crystallization and melting kinetics that are solved numerically for various velocities/undercoolings. The authors conclude that the results for crystallization are qualitatively consistent with models of collision-limited growth kinetics. However, as in the DFT model of Mikheev and Chernov, the absolute rates of crystallization for the LJ system derived by Shen and Oxtoby are found to be significantly smaller than the MD results of Broughton, Gilmer, and Jackson.

C. Kinetic anisotropy

The present results yield the following kinetic anisotropy values for FBD-EAM Ni: $\mu_{100}/\mu_{110} = 1.40 \pm 0.12$ and $\mu_{100}/\mu_{111} = 1.49 \pm 0.26$. The ordering of μ with crystallographic orientation, namely $\mu_{100} > \mu_{110} > \mu_{111}$, is consistent with all previous MD results for fcc-based systems. It has been pointed out by several authors[17,23,24] previously that this ordering is inconsistent with the commonly suggested scaling of the kinetic coefficient with crystalline interplanar spacing d_{hkl}, since for fcc crystals $d_{111} > d_{100} > d_{110}$.

Huitema *et al.*[17] have suggested recently that the fast growth of {100} relative to both {111} or {110} interfaces results from a unique feature of the equilibrium density profile for this orientation. For {100} interfaces it is known that the interlayer spacing increases from a value of d_{100} in the solid to d_{111} near the bulk liquid.[75] Huitema *et al.* show that this interlayer expansion counteracts the decrease in particle density accompanying the transition from solid to liquid, resulting in a roughly constant number of particles ''per layer'' through the interface. This situation for {100} is in contrast with both {110} and {111} orientations where interlayer spacings remain roughly constant,[17,75] and the number of particles per layer decreases with distance across the interface. From interlayer particle fluxes derived by MD, Huitema *et al.* estimate that barriers to interlayer ''hopping'' account for a significant contribution to the overall magnitude of μ in the growth of {110} and {111} interfaces. This contribution is estimated to be significantly reduced for {100} due to the relative absence of variations in the number of atoms per layer across such interfaces. For fcc-based systems the interlayer-expansion effect for {100} interfaces appears to be quite general, having been observed for Lennard-Jones,[17,75] hard-sphere,[76] EAM-Ni,[51] and EAM-Al[77] systems. With the same FBD-EAM Ni potential considered here, a detailed analaysis of the structure of {100} and {111} solid-liquid interfaces was performed by Chen, Barnett, and Landman.[51] These authors report results for the variation of particle number per layer across these interfaces that are very similar to those obtained by Huitema *et al.* for the Lennard-Jones system. The model of Huitema *et al.* offers a plausible explanation for the fast growth of {100} interfaces in fcc-based systems. The model is, however, unable to account for the observation of the substantially lower values of μ_{111} relative to μ_{110} commonly observed from simulations.[10,17,19,23,24]

As discussed above, Burke, Broughton, and Gilmer[10] have proposed that the slow growth of {111} interfaces relative to {100} arises from the presence of stacking-fault defects at the junction of fcc and hcp (hexagonal-close-packed) islands which must anneal away for the {111} interface to advance. The ''stacking-fault-drag'' effect identified by Burke *et al.* is expected to be strongest for systems with low values of the SFE, where high concentrations of defective hcp islands may be expected at the solid-liquid interface. In the present study we have considered a potential for Ni which yields a SFE of approximately 45 mJ/m^2 which is at least an order of magnitude larger than the value for Lennard-Jones and a factor of 5 larger than Au. Consistent with this higher SFE value, we find a value of $\mu_{100}/\mu_{111} = 1.49$ for Ni that is substantially smaller than the values of 2.0–3.6 reported for Lennard-Jones[10,17] and Au.[23,24]

An alternative framework for understanding the origin of μ anisotropy is offered by the kinetic DFT formulation of Mikheev and Chernov.[66] In the Mikheev and Chernov formulation, anisotropy in μ originates from the geometrical projection upon the growth direction of density waves with wave vectors $\{G_1\}$ corresponding to the minimal reciprocal lattice vectors of the crystal. For fcc-based crystals the theory of Mikheev and Chernov predicts values for kinetic anisotropies of $\mu_{100}/\mu_{110} \approx 1.41$ and $\mu_{100}/\mu_{111} \approx 1.29$. It is interesting to note that the Mikheev and Chernov model correctly predicts fastest growth for {100} orientations despite the fact that the interlayer-expansion effect identified by Huitema *et al.*[17] is not explicitly incorporated into the theory. The DFT model also yields values for the ratio μ_{100}/μ_{110} consistent with the present and previous simulation results. For the Lennard-Jones and Au systems, the Mikheev and Chernov model underestimates the magnitude of $\mu_{100}/\mu_{111} \approx 2.0$–3.6

derived by MD.[10,17,19,23,24] This discrepancy may in part reflect the stacking-fault-drag effect discussed above, which is not explicitly accounted for in the DFT model. For Ni, our present MD result, $\mu_{100}/\mu_{111}=1.49$, shows a trend towards improved agreement with the Mikheev and Chernov prediction with increasing SFE. At present it remains unclear why the Mikheev and Chernov model appears to be reasonably accurate for predicting kinetic anisotropy while underestimating the overall magnitude of μ (see above).

V. SUMMARY

The results of the present NEMD study of the kinetic coefficient in elemental Ni can be summarized as follows.

(1) Using the EAM Ni potential of Foiles, Baskes, and Daw, we obtain the following orientation-dependent values of the kinetic coefficient: $\mu_{100}=35.8\pm2.2$, $\mu_{110}=25.5\pm1.6$, and $\mu_{111}=24.1\pm4.0$ in units of cm/s K. The associated kinetic anisotropies are thus calculated to be $\mu_{100}/\mu_{110}=1.40\pm0.12$ and $\mu_{100}/\mu_{111}=1.49\pm0.26$. The present results are demonstrated to be relatively insensitive to the choices of system size and thermostat/piston-mass variables employed in the NEMD simulations.

(2) Our results feature highly symmetric melting and growth kinetics in the regime of low undercoolings explored in this work. These results are thus in agreement with those of Tepper and Briels for the Lennard-Jones system,[21] while they are qualitatively different from the asymmetric melting and growth kinetics obtained with MD by Tymczak and Ray[11,12] for Na and Celestini and Debierre[23] for Au.

(3) In comparison to previous studies for related fcc-based systems, we find a number of differences in the kinetics of {111} interfaces. Specifically, our results for μ_{111} are found to be relatively insensitive to size of the MD simulation cell. Further, the anisotropy μ_{100}/μ_{111} calculated for the Ni potentials of Foiles-Baskes and Daw [1.49(23)] is substantially smaller than related values of 2.0–3.6 derived for the low-SFE Lennard-Jones[10,17] and Au (Refs. 23 and 24) systems.

(4) The Broughton-Gilmer-Jackson[9] model for collision-limited growth yields predictions for μ_{100} in reasonably good agreement with the present Ni results. The DFT model of Mikheev and Chernov[66] underestimates by approximately 25% the magnitudes of μ derived here, while producing estimates for kinetic anisotropy that are consistent with the present results.

ACKNOWLEDGMENTS

This research was supported by the U.S. Department of Energy, Office of Basic Energy Sciences, under Contracts Nos. DE-FG02-01ER45910 (D.Y.S., M.A. and J.J.H.) and DE-FG02-92ER45471 (D.Y.S.), as well as the DOE Computational Materials Science Network program. Use was made of resources at the National Energy Research Scientific Computing Center, which is supported by the Office of Science of the Department of Energy under Contract No. DE-AC03-76SF00098. We gratefully acknowledge helpful discussions with Professor Alain Karma and Professor Franck Celestini.

*Permament address: Institute of Solid State Physics, Academia Sinica, 230031-Hefei, China.

[1] R. Willnecker, D.M. Herlach, and B. Feuerbacher, Phys. Rev. Lett. **62**, 2707 (1989).

[2] J.W. Lum, D.M. Matson, and M.C. Flemings, Metall. Mater. Trans. B **27B**, 865 (1996).

[3] K. Eckler, F. Gärtner, H. Assadi, A.F. Norman, A.L. Greer, and D.M. Herlach, Mater. Sci. Eng., A **226-228**, 410 (1997).

[4] D.M. Matson, in *Solidification 1998*, edited by S.P. Marsh, J.A. Dantzig, R. Trivedi, W. Hofmeister, M.G. Chu, E.J. Lavernia, and J.-H. Chun (The Mineral, Metals and Materials Society, Warrendale, PA, 1998), p. 233.

[5] W.J. Boettinger, S.R. Coriell, A.L. Greer, A. Karma, W. Kurz, M. Rappaz, and R. Trivedi, Acta Mater. **48**, 43 (2000).

[6] J. Bragard, A. Karma, Y.H. Lee, and M. Plapp, Interface Sci. **10**, 121 (2002).

[7] M.E. Glicksman and R.J. Schaefer, J. Cryst. Growth **1**, 297 (1967).

[8] G.H. Rodway and J.D. Hunt, J. Cryst. Growth **112**, 554 (1991).

[9] J.Q. Broughton, G.H. Gilmer, and K.A. Jackson, Phys. Rev. Lett. **49**, 1496 (1982).

[10] E. Burke, J.Q. Broughton, and G.H. Gilmer, J. Chem. Phys. **89**, 1030 (1988).

[11] C.J. Tymczak and J.R. Ray, Phys. Rev. Lett. **64**, 1278 (1990).

[12] C.J. Tymczak and J.R. Ray, J. Chem. Phys. **92**, 7520 (1990).

[13] C.F. Richardson and P. Clancy, Mol. Simul. **7**, 335 (1991).

[14] C.F. Richardson and P. Clancy, Phys. Rev. B **45**, 12 260 (1992).

[15] R. Moss and P. Harrowell, J. Chem. Phys. **100**, 7630 (1994).

[16] W.J. Briels and H.L. Tepper, Phys. Rev. Lett. **79**, 5074 (1997).

[17] H.E.A. Huitema, M.J. Vlot, and J.P. van der Eerden, J. Chem. Phys. **111**, 4714 (1999).

[18] H.E.A. Huitema, B. van Hengstum, and J.P. van der Eerden, J. Chem. Phys. **111**, 10 248 (1999).

[19] J.J. Hoyt, B. Sadigh, M. Asta, and S.M. Foiles, Acta Mater. **47**, 3181 (1999).

[20] H.L. Tepper and W.J. Briels, J. Cryst. Growth **230**, 270 (2001).

[21] H.L. Tepper and W.J. Briels, J. Chem. Phys. **115**, 9434 (2001).

[22] H.L. Tepper and W.J. Briels, J. Chem. Phys. **116**, 5186 (2002).

[23] F. Celestini and J.-M. Debierre, Phys. Rev. E **65**, 041605 (2002).

[24] J.J. Hoyt and M. Asta, Phys. Rev. B **65**, 214106 (2002).

[25] J.J. Hoyt, M. Asta, and A. Karma, Interface Sci. **10**, 149 (2002).

[26] K.A. Jackson, Interface Sci. **10**, 159 (2002).

[27] K.A. Jackson and B. Chalmers, Can. J. Phys. **34**, 473 (1956).

[28] H.A. Wilson, Philos. Mag. **50**, 238 (1900).

[29] J. Frenkel, Phys. Z. Sowjetunion **1**, 498 (1932).

[30] D. Turnbull and B.G. Bagley, Solid State Chem. **5**, 526 (1975).

[31] S.R. Coriell and D. Turnbull, Acta Metall. **30**, 2135 (1982).

[32] M.S. Daw and M.I. Baskes, Phys. Rev. Lett. **50**, 1285 (1983).

[33] M.S. Daw and M.I. Baskes, Phys. Rev. B **29**, 6443 (1984).

[34] S.M. Foiles, M.I. Baskes, and M.S. Daw, Phys. Rev. B **33**, 7983 (1986).

[35] A.F. Voter and S.P. Chen, in *Characterization of Defects in Materials*, edited by R.W. Siegel, J.R. Weertmann, and R. Sinclair, Mater. Res. Soc. Symp. Proc. **82** (Materials Research Society, Pittsburgh, 1987), p. 175.

[36] In our previous work for Ni, values of μ for low undercoolings were estimated by extrapolating nonlinear velocity vs undercooling data from relatively high temperatures. Due to relatively large statistical scatter in our previous data, this procedure represents a potential source of uncertainty in our estimated values for μ anisotropy for low interface velocities.
[37] S.M. Foiles, Phys. Rev. B **32**, 3409 (1985).
[38] J.R. Morris, C.Z. Wang, K.M. Ho, and C.T. Chan, Phys. Rev. B **49**, 3109 (1994).
[39] J.R. Morris and X.Y. Song, J. Chem. Phys. **116**, 9352 (2002).
[40] D. Alfé, M.J. Gillan, and G.D. Price, J. Chem. Phys. **116**, 6170 (2002).
[41] S.M. Foiles and M. Daw, computer code DYNAMO (Sandia National Laboratories, unpublished).
[42] S.J. Plimpton and B.A. Hendrikson in *Materials Theory and Modeling*, edited by J. Broughton, P.D. Bristowe, and J.M. Newsam, Mater. Res. Soc. Symp. Proc. No. **291** (Materials Research Society, Pittsburgh, 1993), p. 37.
[43] M.P. Allen and D.J. Tildesley, *Computer Simulation of Liquids* (Clarendon Press, Oxford, 1993).
[44] S. Nosé, J. Chem. Phys. **81**, 511 (1984); Mol. Phys. **52**, 255 (1984).
[45] W.G. Hoover, Phys. Rev. A **31**, 1695 (1985); **34**, 2499 (1986).
[46] H.C. Andersen, J. Chem. Phys. **72**, 2384 (1980).
[47] M. Parinello and A. Rahman, Phys. Rev. Lett. **45**, 1196 (1981).
[48] M. Parinello and A. Rahman, J. Appl. Phys. **52**, 7182 (1981).
[49] M. Parinello and A. Rahman, J. Chem. Phys. **76**, 2662 (1982).
[50] S.M. Foiles and J.B. Adams, Phys. Rev. B **40**, 5909 (1989).
[51] E.T. Chen, R.N. Barnett, and U. Landman, Phys. Rev. B **40**, 924 (1989).
[52] In the default fixed-pressure dynamics in the DYNAMO and PARADYN codes an additional term of the form $-\beta\dot{L}_\alpha$ is added to the right-hand side of Eq. (3). The additional boundary drag term β has the effect of siginificantly decreasing the equilibration time in a constant-pressure simulation, but $\beta \neq 0$ is inappropriate for free solidification simulations. At a constant crystallization rate, $\ddot{L}_\alpha = 0$ and $\dot{L} = \text{const}$, meaning the pressure will equilibrate at some value other than the desired pressure P_α^0 and thus the undercooling will be altered. In all simulations reported here we employ standard Parinello-Raman dynamics with no boundary drag term.
[53] Y.G. Chusak and L.S. Bartell, J. Phys. Chem. **105**, 11 605 (2001).
[54] F. Baletto, C. Motter, and R. Ferrando, Chem. Phys. Lett. **354**, 82 (2002).
[55] O.R. de la Fuente and J. Soler, Phys. Rev. Lett. **81**, 3159 (1998).
[56] *Smithell's Metals Reference Book*, edited by E.A. Brandes (Butterworths, Boston, 1983).
[57] M. Asta, D.Y. Sun, and J.J. Hoyt, in *Thermodynamics, Microstructure and Plasticity*, Vol. 108 of *NATO Advanced Studies Institute, Series II: Mathematics, Physics, and Chemistry*, edited by A. Finel, D. Mazière, and M. Veron (Kluwer Academic Publisher, Norwell, MA, 2003).
[58] D.R. Uhlmann, J.F. Hays, and D. Turnbull, Phys. Chem. Glasses **8**, 1 (1967).
[59] It is also interesting to note that the simulation cells employed in these simulations featured asymmetric boundary conditions with liquid-vapor and one solid-vapor interface on either end of the box.
[60] F. Ercolessi, M. Parinello, and E. Tossatti, Philos. Mag. A **58**, 213 (1988).
[61] F. Celestini, F. Ercolessi, and E. Tosatti, Phys. Rev. Lett. **78**, 3153 (1997).
[62] A.E. Carlsson, Solid State Phys. **43**, 1 (1990).
[63] F. Celestini (private communication).
[64] A. Karma, Phys. Rev. Lett. **70**, 3439 (1993).
[65] A. Karma, Phys. Rev. E **48**, 3441 (1993).
[66] L.V. Mikheev and A.A. Chernov, J. Cryst. Growth **112**, 591 (1991).
[67] S.A. Schofield and D.W. Oxtoby, J. Chem. Phys. **94**, 2176 (1991).
[68] H. Löwen, S.A. Schofield, and D.W. Oxtoby, J. Chem. Phys. **94**, 5685 (1991).
[69] H. Löwen and J. Bechoefer, Europhys. Lett. **16**, 195 (1991).
[70] D.W. Oxtoby and P.R. Harrowell, J. Chem. Phys. **96**, 3834 (1992).
[71] Y.C. Shen and D.W. Oxtoby, J. Chem. Phys. **104**, 4233 (1996).
[72] E.G.D. Cohen, P. Westerhuijs, and I.M. de Schepper, Phys. Rev. Lett. **59**, 2872 (1987).
[73] W.A. Curtin and N.W. Ashcroft, Phys. Rev. Lett. **56**, 2776 (1986).
[74] R. Ohnesorge, H. Löwen, and H. Wagner, Phys. Rev. A **43**, 2870 (1991).
[75] J.Q. Broughton and G.H. Gilmer, J. Chem. Phys. **84**, 5749 (1986).
[76] R.L. Davidchack and B.B. Laird, J. Chem. Phys. **108**, 9452 (1998).
[77] B.B. Laird (private communication).